sciendo

PRODUCTION ENGINEERING ARCHIVES 2025, 31(4), 517-525

PRODUCTION ENGINEERING ARCHIVES

ISSN 2353-5156 (print)
ISSN 2353-7779 (online)

Exist since 4th quarter 2013
Available online at https://pea-journal.eu

Design and evaluate a customized PEEK implant for large skull defect reconstruction

Waad Q. Shiaa[1*], Rasha Jabbar[1], Samah A. Aufy[1]

[1] Industrial and Systems Engineering Department, College of Production Engineering and Metallurgy, University of Technology - Iraq, Baghdad, Iraq; waad.q.shiaa@uotechnology.edu.iq (WQS); Rasha.J.Alasadi@uotechnology.edu.iq (RJ); Samah.A.Alkhalidy@uotechnology.edu.iq (SAA)
*Correspondence: waad.q.shiaa@uotechnology.edu.iq

Article history
Received 31.07.2025
Accepted 03.11.2025
Available online 12.12.2025

Keywords
Computer-aided design,
Customized implant,
Finite element analysis,
Additive manufacturing,
PEEK.

Abstract
Rehabilitation of the cranium's bones is considered a complicated procedure that presents a challenge to the surgical staff. Typically, the primary focus when designing an implant should involve selecting optimal design techniques and materials. Material and design should provide a strong, comfortable, simple-to-fit, and attractive implant. Therefore, this study aims to design a suitable customized PEEK implant. Initially, 3D models of the damaged region were created using interactive CAD modelling techniques. While creating the implant model used mirror-based reconstruction. Furthermore, finite element analysis was implemented to evaluate the implant's stability and structural strength. Then morphological analysis was used to assess the precision of virtual fitting. Finally, fused filament fabrication was used to manufacture it. Under simulation, the implant was subjected to a constant load of 50 Newtons and intracranial pressures. According to the simulation results, the maximum Von Mises stress was about 22.057E-2 MPa, the Von Mises strain was 5.8135E-5, and the deformation was 1.9103 µm. That means the maximum recorded stress is quite low in comparison with the material's yield strength. This reflects the ability to endure and maintain safety of the studied implant. While the morphological test showed that the exterior profile curvature contours were uniformly reconstructed, maintaining contiguity between the implant and the skull model, which indicates a suitable fit.

DOI: 10.30657/pea.2025.31.48

1. Introduction

Cranium defects become more frequent due to increased traffic collisions, tumours, and calamities, thus increasing the demand for cranium repair (Obaeed & Hamdan, 2024). Cranial abnormalities reconstruction is a great challenge to surgeons due to the particular cranial anatomy. The first step to solving cranial issues involves the correction of displaced cranial bones and their replacement with adequate implants to regain functionality (Mandolini et al., 2019). The complex operation of treating large cranial defects was previously complicated by the requirement for hand manipulation with the use of two-dimensional (2D) imaging. This involved the shaping, modeling, and adjusting of the implant (of bone transplant, bone cement, or titanium mesh). This conventional technique led to complexity with unpleasing final aesthetic results. These methods evolved from manual shaping and casting-based techniques to use computer-aided design (CAD) and computer-aided manufacturing (CAM) (Bhargava et al., 2010). This enabled the use of new materials in production, resulting in better overall quality and improved follow-up results. Three-dimensional (3D) printing has remarkably revolutionized the production of medical prostheses. 3D printing, also known as additive manufacturing (AM), builds 3D objects by sequentially layering material (Al-Wswasi et al., 2025; Mansor et al., 2024). The technology of 3D printing has dramatically improved the ability to create objects with complex geometries that cannot be made through traditional methods—a development particularly felt in the health care field (Neamah et al., 2024). Medical imaging data from computed tomography (CT) or magnetic resonance imaging (MRI) scans can be used for a 3D rebuilding of the human anatomy (Shiaa et al., 2024a). Next, implants can be designed to fit these models perfectly. In designing cranial prostheses, these two factors should receive the most consideration, i.e., biocompatibility and patient-specific customization. The appropriate use of materials guarantees biocompatibility. The analysis of diagnostic imaging data acquired from patients enables customization.

Such data allows the accurate representation of skull injury and the associated skeletal structures. Implants are then tailored to create the anatomy of each patient (Shiaa et al., 2023). There are usually two main design types for a skull injury repair based on the complexity of the skull injury:

- Mirrored reconstruction: This technique is based on the symmetry of bones and is the most effective when used on single skeletal injuries on the cranium (Kung et al., 2020). Cranial symmetry is the principle behind reconstructing the missing bone segment using the mirrored healthy cranium from the other side. The advantage of this technology is its capacity to generate a customized cranial implant with a thickness that perfectly corresponds to that of the cranial bone (Moiduddin et al., 2017). However, a significant limitation of the approach is its inapplicability to asymmetrical body areas. If the defect is located in the center of the cranium, the approach is unable to offer a healthy alternative.
- Anatomical reconstruction: This method involves modifying the surface shape by selecting two curves from the areas that were removed and using a reference curve to rebuild the bone structure (Harrysson et al., 2007). The primary advantage is its applicability in both symmetrical and asymmetrical areas. However, complex-shaped regions need technical proficiency.

Recent studies have focused on the implantation of bone tissue with alternative materials. Titanium (Ti) and its alloys have been widely used for decades in this field as a biocompatible metal material. The commonest biomaterial used for implant reconstructions is titanium alloy (Ti6Al4V). They provide several benefits, including enhanced biocompatibility, excellent mechanical properties, osseointegration capabilities, significant corrosion and wear resistance, and high strength (Trevisan et al., 2018). However, Ti is characterized by its high density, quick heat conduction, and absorption. Consequently, Ti is not appropriate for the replacement of bone tissue that is susceptible to thermal sources. Other drawbacks of Ti include its incompatibility with modern imaging technology, its difficulty in processing, and its aesthetically unappealing colour difference from human bone in thin-skin areas. Additionally, titanium has a significantly larger modulus of elasticity in comparison to bone. The substantial discrepancy between the two often leads to implant failure due to the long-term effects of stress shielding (Lee et al., 2012). Moreover, metallic implants subjected to radiation produce scattering rays that adversely affect tissues. Consequently, studies have focused on evaluating possible Ti alternatives that can reduce the aforementioned limitations and decrease biological complications following implant insertion.

Biomaterials such as ceramics and polymers have been studied as craniofacial restoration alternatives to metals. Polymers are particularly appealing for craniofacial repairs because of their favorable processability and cost-effectiveness relative to metals and ceramics. In contrast to ceramics, which exhibit brittleness, these materials demonstrate resilience. Furthermore, unlike metallic implants that may produce imaging artefacts, polymers are radiolucent, which allows for an unhindered postoperative clinical diagnosis (Jindal et al., n.d.). Table 1 describes the mechanical properties of the primary biomaterials used in cranium repair, namely titanium (Ti), polymethyl methacrylate (PMMA), and polyether ether ketone (PEEK). Additionally, it contains the characteristics of actual skull bone. PMMA was among the initial synthetic materials used in biological applications and is also utilized in cranioplasty. Furthermore, PMMA has a superior transplant success rate compared to Ti alloy (Lalegani Dezaki et al., 2021). However, PMMA implants have inadequate osseointegration characteristics (de Souza Leão et al., 2018). Furthermore, the unrefined methyl methacrylate constituent in PMMA comprises irritants (Becker et al., 2011). These factors lead to an increased need for biocompatible high-performance polymers like PEEK in skull repairs and orthopaedic surgeries. These materials are chemical-resistant, heat-resistant, and bone-like, making them a suitable surgical option for craniofacial reconstruction compared to metal components. It is also compatible with medical imaging to assess fracture progression. Moreover, it is lightweight and has elasticity nearly that of human bone, in contrast to Ti, hence reducing stress concentration around the implant. In comparison to PMMA, it also has a high level of chemical and biological resistance, which reduces the probability that the body will react to the material. Therefore, PEEK material can be considered a more suitable material for implants to be able and endure physiological loads while maintaining biocompatibility (Punchak et al., 2017). Two common 3D printing processes for PEEK are fused filament fabrication (FFF) and selective laser sintering (SLS). In SLS, the powder is made to flow and is melted by a laser or electron beam to sinter the powder into a solid, as shown in Fig. 1. In contrast, the FFF printing process is when the filament is advanced to the printer with the aid of the feed drive. The process involves heating the material to the point of near-liquefaction, which is then extruded through a nozzle. The object is later on built over a printing bed in an incremental manner (Al-Bdairy et al., 2025; Jabbar et al., 2020; Saleh et al., 2025). This is achieved with specially developed medical-grade PEEK filaments and high-temperature FFF 3D printers for medical PEEK applications. In comparison with the SLS process, the FFF process is more attractive for its low initial capital investment, easy operation, and healthier workspace (Singh et al., 2019). However, there are still many difficulties in this method, such as temperature adjustment during the printing of PEEK, residual stress accumulation, and anisotropy of 3D-printed FFF PEEK implants. Furthermore, PEEK is susceptible to warping and partial crystallization, which have a negative influence on the mechanical performance of the part (Zanjanijam et al., 2020). As a result, fundamental FFF processing parameters, like nozzle, chamber, print speed, and bedplate temperature, should be optimized to improve layer bonding and achieve the best results.

Recently, many studies have been devoted to the study of 3D-printed PEEK. (Petersmann et al., 2023) tested its print quality and mechanical strength at various build orientations (BO) and temperatures of airflow (AF). High mechanical strength is seen in prostheses printed in a horizontal orientation (BO 180°). The surface quality was good for BO 90°, but

Table 1. Mechanical characteristics of primary materials important for skull rebuilding (Luo et al., 2023).

Material	Young's modulus	Ultimate tensile strength	Poisson's ratio	Density
-	GPa	MPa	-	g/cm^3
Ti alloy	110	1300	0.30	4.42
PMMA	3.0	72	0.38	1.18
PEEK	3.5	105	0.40	1.30
Cranial bone	5.38	43	-	1.80

only fair for BO 180º. Increased crystallinity and even color distribution, however, were associated with increased AF levels. (Liu et al., 2023) a mechanical study was performed to evaluate the effectiveness of PEEK skull implants manufactured by powder bed fusion (PBF) and FFF. The results show that the FFF prosthesis absorbed more energy during compressive tests and impact tests than the PBF prosthesis. (Sonaye et al., 2025) studied the influence critical FFF 3D printing parameters have on the mechanical and material properties of skull PEEK prostheses and on their impact resistance. The tests demonstrated that specimens printed at 0°BO, under ideal printing conditions, had an ultimate load of 2034 N. Furthermore, computational simulations, such as FEA, have become indispensable in the field of healthcare engineering and the assessment of the integrity of skull reconstruction. FEA allows for mechanical strength and impact resistance analysis while pointing out the stress concentration in cranial implants without conducting physical testing. Consequently, the outcomes of the assessments can be applied to the development of prostheses. (Huys et al., 2021) investigated the design for three patient-specific cranium implants by FEA. The study comprised one PEEK cranial implant secured with tangential screws and two ceramic-titanium cranial implants secured with tangential or axial screws. The results indicate that the implant material and fixation method have significant influences not only on the location but also on the amount and distribution of stresses. (Moncayo-Matute et al., 2023) described the behavior of the implant to forces from the outside using FEA with PMMA and PEEK materials. This article discusses the economic advantages of PMMA in relation to PEEK. (Mejía Rodríguez et al., 2024) investigated PMMA and PEEK cranial prosthesis for the relationship between their thickness and displacement. The results support that PMMA implants with a thickness of approximately 4 mm, including perforations, would be an economic alternative to PEEK prostheses.

Numerous efforts have introduced significant progress in the recent past. However, further study is required to fully evaluate the biocompatibility and anatomical precision of the implants produced for the reconstruction of large defects. In addition, evaluating the implants for natural working conditions and analyzing their compatibility with the surrounding bone structure is crucial to obtaining a favorable clinical result. Therefore, the aim of this study is to present a method for designing a patient-specific prosthesis and evaluate the accuracy of its virtual fitting. Initially, a numerical model of the skull, with a defective area, was created using an interactive CAD modelling technique. After that, the geometry of the implant was designed using a mirror-based reconstruction method. Furthermore, the method used FEA to evaluate the implant's strength and compare the distribution of stress and displacements, besides a morphological analysis to determine its accuracy. A PEEK cranial implant was finally fabricated using FFF technology.

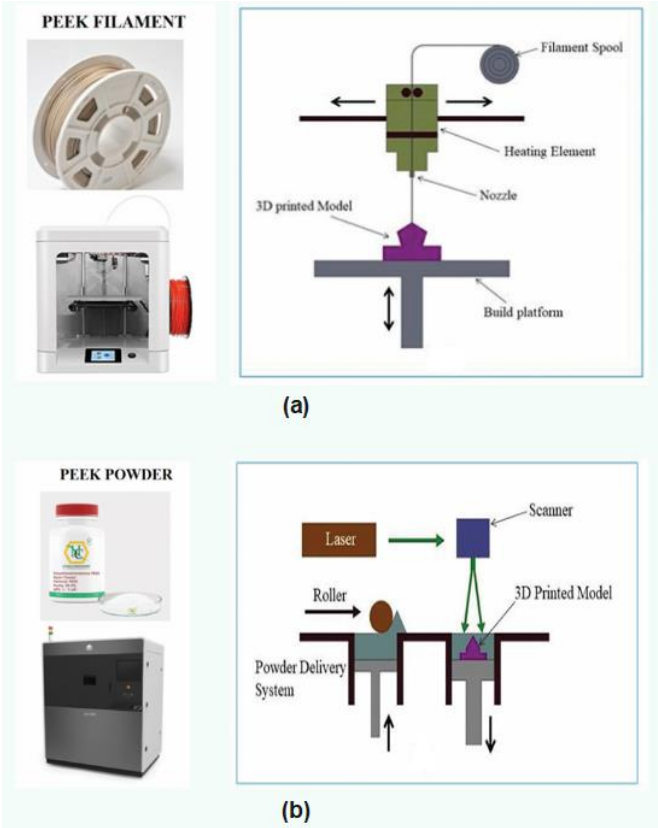

Fig. 1. Various 3D printing techniques for the manufacture of PEEK implants. a) FFF and b) SLS.

2. Materials and methods

The process of designing a cranial implant involves four primary steps: rebuilding the 3D skull model, creating the cranial implant, attaching fixation components, and evaluating the design through simulation. Figure 2 illustrates the total progression of the design. A skull prosthesis is created from a 3D model and stored in standard tessellation language (STL) format. CT scans are used to gather the patient's 3D images, which include details on their bones, muscles, skin, brain, and other organs (Shiaa et al., 2024b). For cranial patching, a segment of the cranial bones is removed from these 3D pictures. Following the creation of a 3D CAD model of the patient's cranial defect, reverse engineering was used to create the skull implant, utilizing the mirrored reconstruction approach. The strength and suitability of the design have been assessed by using simulation findings. Lastly, 3D printing is used to produce customized skull implants, which help a surgeon with preoperative planning by confirming the accuracy of the implant's design and aesthetics.

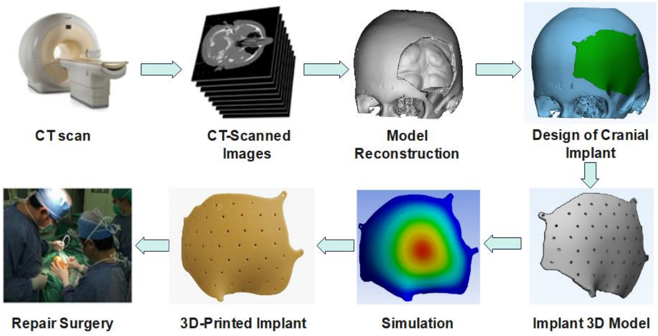

Fig. 2. Flowchart for skull reconstructive surgery

2.1. Acquisition of data and processing

This article includes an examination at a case study from Saad Al Watary Neurological Sciences Hospital involving a patient who needed skull plates replaced. The patient had injuries in an accident, leading to a significant post-traumatic deformity in the left frontal bones. The significant bone defect was due to a decompressive craniotomy. Skull reconstruction was necessary for re-establishing the patient's facial attractiveness and the cranium's structural integrity. The skull of a patient was scanned using a CT. The CT scan images were saved as DICOM (Digital Imaging and Communications in Medicine) formats. The DICOM data architecture consists of 467 slices, each with a depth of 0.3 mm. The DICOM file containing the 2D image layers obtained by the CT scan was loaded into Mimics, a medical image processing program. Subsequently, a region of growing selection was conducted, using the built-in greyscales. Semiautomatic segmentation algorithms built into the program were used to create a 3D volumetric model of the cranial structure. Figure 3 depicts the completed segmentation process from a completely imaged cranial to the targeted area of interest, namely the 3D cranial model (defect zone), excluding the neck and mandible. The 3D cranial model was preserved in the STL file format for the subsequent cranial implant modelling procedure.

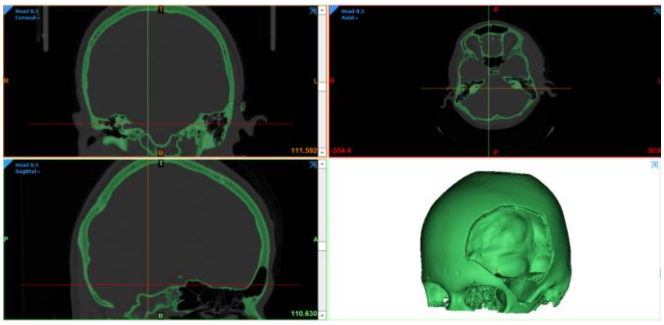

Fig. 3. Processing images to create a 3D volumetric model of the patient's skull**.**

2.2. 3D modelling and designing processes

The primary aim of this stage was to create a customized implant for the patient's cranium. The STL file of the 3D volumetric rebuilt model (Fig. 4a) was loaded into a medically approved CAD modelling program, 3-matic. A mirror-based reconstruction method was used for the restoration of the skull damage. Initially, a mid-plane reference was determined, and the unaffected side was mirrored onto the affected side. For precise alignment and obtaining the outlines for implant rebuilding, the reflected side was matched with the surrounding bone on the affected side (Fig. 4b). Afterwards, a curve was designed to indicate the defect boundary using curvature analysis (Fig. 4c). To ensure tangency across the implant and the cranial bone, it is crucial to delineate the curve around the anatomical defect in regions of low curvature. Following that, three equidistant sketch graphs were positioned perpendicularly to the datum plane at various locations inside the cranial model (Fig. 4d). The contours derived from the intended curvature of the unaffected and mirrored skull model were transferred into the individual designs, serving as reference planes for implant construction. The primary objective was to utilize those reference planes as anatomic limitations in determining the points for the thin-plate spline (TPS) approach (Fig. 4e). The TPS method interpolates and guesses absent data using comparable reference points found in the mirrored and defective cranial model. Lastly, an internal coordinate system method predicated on anatomic-controlled deformation was used to produce the implant shape with a tapering edge that overlaps the adjacent bone. A "surface/triangle normal" or inward-directed lowering surgery was then executed on the implant to eliminate any impediments to its matching onto the skull model (Fig. 4f). The customized implant was ultimately preserved and exported in STL file format for additional modelling.

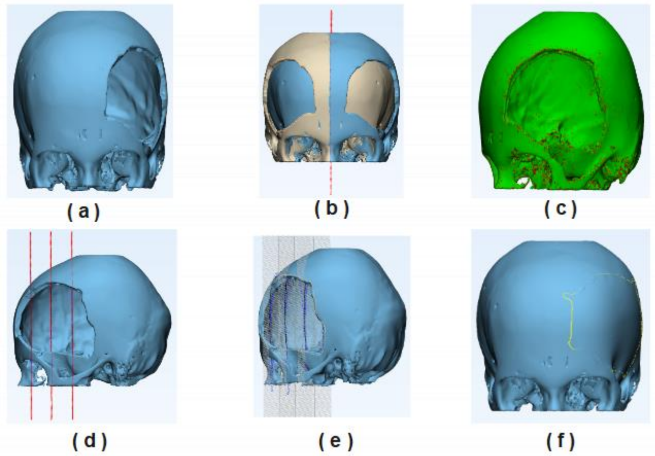

Fig. 4. The process of designing a skull implant is illustrated schematically. a) a 3D cranial model, b) establish a datum plane and reflect the unaffected side onto the defective side, c) analyze and optimize the curvature of a curve, d) sketch graphs with equal spacing that are vertical to the datum plane, e) form splines, and f) rebuild the skull using a cranial implant.

2.3. Design fixation parts

In order to secure the implant to the skull, it was necessary to include fixation components in the design of the implant. According to the patient's skull anatomy and deliberation with the surgeon, the skull implant was digitally designed with the fixation pieces' location, form, and size in mind. Throughout the implant's perimeter, fixation components were dispersed in accordance with the principal design criteria, which called for their placement on the thicker skull bone away from any nerve locations. A minimum of three fixation components is required for big skull implants to assist in the process of securing the implant on the patient's skull. For optimal contact zone and aesthetics, the fixation components were placed tangent to the cranium. Figure 5a shows the 3D model after cylindrical screws were inserted. The screw should be of an appropriate length so it does not irritate the meninges, which is essential for the patient's safety. As a result, the screw is 2 millimeters in diameter and 4 millimeters in depth. Finally, the implant design with holes/openings was generated to soft tissue interconnect, as shown in Fig. 5b.

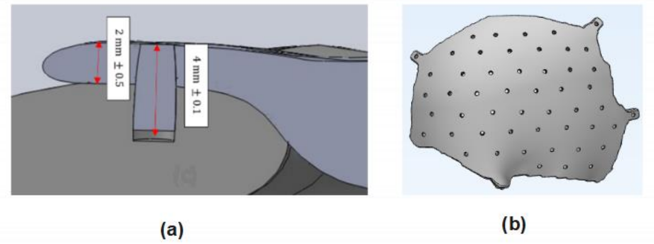

Fig. 5. a) Fastening screws skull implant. b) Cranial implant with fixation parts.

2.4. Finite element model

All phases of the FEA process were executed with the Ansys® Mechanical program. For this analysis, a solid geometry was generated using the STL model of the skull implant acquired. The mesh produced by 3Matic was corrected, smoothed, and homogenized using Ansys®'s SpaceClaim tool to provide an appropriate model for simulation. Subsequently, the solid model was produced through the process schematic shown in Fig. 6. Initially, 12 manually created patches were used to recreate the implant's curvature (Fig. 6b). The second step was to combine the 12 patches into one surface (Fig. 6c). Next, a solid model was obtained by offsetting the surface (Fig. 6d). Lastly, the model was utilized to create the 2 mm-diameter holes that were used to secure the implant (Fig. 6e, f).

FEA testing is run on the computational model in a static structural setting. For the case under study, the material properties of cranial bone and PEEK are assumed to be isotropic. In literature, the mechanical properties such as Young's modulus and Poisson's ratio are determined for both PEEK and cranial bone. In particular, the PEEK implant's Young's modulus and Poisson's ratio are determined at 3.5 GPa and 0.4, respectively. The Young's modulus and Poisson's ratio for cranial bones were determined to be 15 GPa and 0.3, respectively (Mejía Rodríguez et al., 2024). The replacement patch undergoes two loads—one on its inside and one on its outside surface. The maximal load, which is 15 mmHg and is comparable to intracranial pressure (Canac et al., 2020), was applied to the whole inner surface of the skull implant. Additionally, an outside force of 50 N was applied, which is equivalent to the mass of the person's head when they are in the lying position (Ridwan-Pramana et al., 2016). The cranium was a stationary component, exhibiting no displacements.

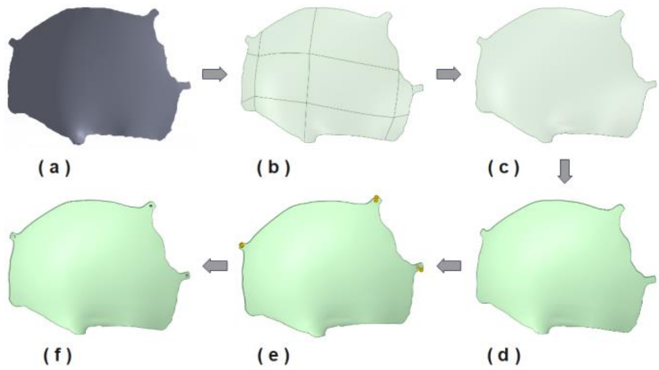

Fig. 6. Illustrates the workflow for generating a solid geometry for FEA. a) Initiate the STL model, b) generate patches, c) combine patches, d) offset the surface, e) generate cylinders for apertures, and f) model apertures for fixation.

3. Results and discussion

3.1. Customized implant structure analysis

This work identified the deformation, von Mises strain, and von Mises stress parameters on the skull implant as criteria. In order to conduct a convergence test, iterative processes is performed with varying mesh sizes, and the change of maximum Von Mises stress with increasing number of elements was analyzed. The observed results indicated that the maximum Von Mises stress remained steady when the number of elements exceeded 29,424, as shown in Fig. 7. Additionally, the error ratio between subsequent meshes was less than 1%, indicating that the numerical convergence test was completed. The mesh with 38486 elements (61233 nodes) is used to achieve a balance between result accuracy and computational processing time. Initially, the FEA model was simulated under intracranial pressure. A typical human body pressure is less than or equal to 15 mmHg. Through this model, a pressure equal to or more than 15 mmHg, or about 2000 Pa (2 E-3 MPa), is applied to the full face, including the bone and implant. Subsequently, the cranial implant and skull are subjected to an outside load of 50 N, equivalent to the mass of the person's head in a lying-down state. Ultimately, an outside force of 50 N and an intracranial pressure of 2000 Pa were implemented. The simulation results, which compare the three cases throughout the three parameters, are presented in Figs 8, 9, and 10, as well as in Table 2.

The findings of the simulation for case 1 involving intracranial pressure are presented in Fig. 8. The implant structure has a deformation value of 5.3363E-4 mm, focused near the implant's center. The implant designs have a very low strain value of 1.7135E-5. An internal edge of the implant has a highest stress value of 6.5007E-2 MPa. Next, a force of 50 N, similar to the mass of a human head, applies through the outer surface to the inside. Figure 9 presents the findings of the second case's simulation. In contrast to case 1, case 2 exhibits significantly elevated deformation, stress, and strain values. The maximal deformation value in this instance is approximately 1.9103E-3 mm and is situated in proximity to the center. The maximum strain value of the implant is approximately 5.8135E-5, while the maximum stress value is 22.057E-2 MPa. Finally, the outcomes from the simulation for case 3, which involved intracranial pressure and an outside force, are presented in Fig. 10. Relative to case 1, the deformation, stress, and strain readings in case 3 are dramatically increased and decreased compared to those in case 2. The highest deformation value is at the outside force's location, about 1.3783E-3 mm. A maximal stress value of 15.557E-2 MPa is observed in this case, with a maximum strain value of approximately 4.1001E-5.

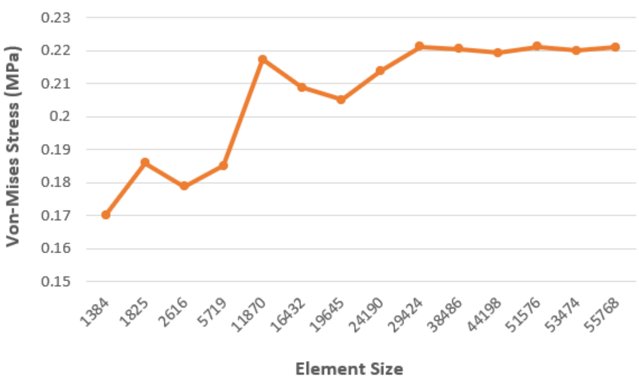

Fig. 7. Maximum Von Mises stress vs. mesh element size.

3.2. A morphological evaluation

The morphological analysis included checking the virtual fit and curve continuity of the implant's design with the cranium. The STL file of the cranial model and the designed implant have been inspected in cross-sectional views across three planes. Figure 11 shows the y-, z-, and x-axis cutting planes for the implant and the skull model, respectively. The cross-sectional analysis demonstrated a high degree of consistency in the external profile curvature curves between the cranial model and the designed implant, as illustrated in Fig. 11. The

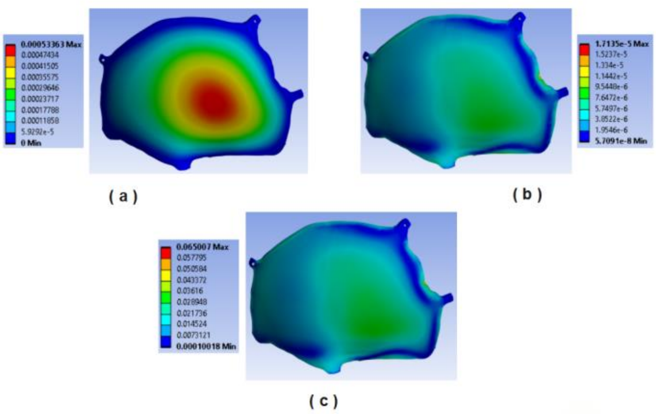

Fig. 8. Maps of case 1: a) Total deformation, b) Von Mises strain, c) Von Mises stress.

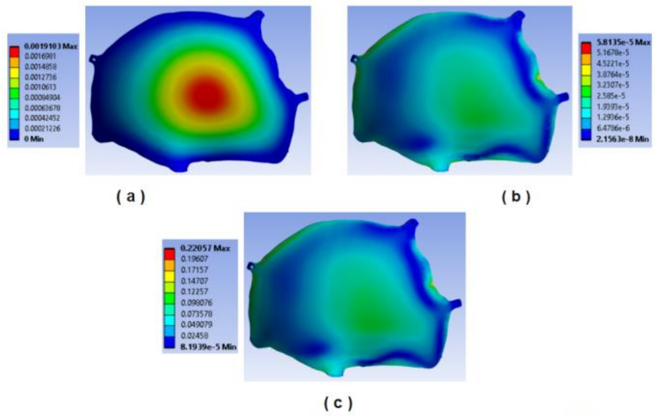

Fig. 9. Maps of case 2: a) Total deformation, b) Von Mises strain, c) Von Mises stress.

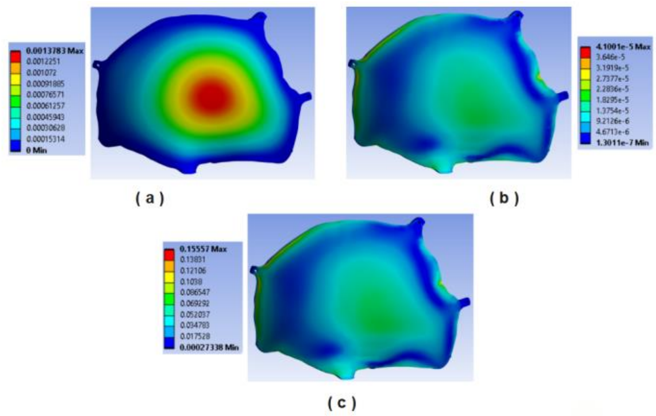

Fig. 10. Maps of case 3: a) Total deformation, b) Von Mises strain, c) Von Mises stress.

Table 2. Simulation results for all cases.

Case		Total deformation (mm)	Von Mises Strain	Von Mises Stress (MPa)
Case 1	Min.	0	5.7091E-8	10.018E-5
	Max.	5.3363E-4	1.7135E-5	6.5007E-2
Case 2	Min.	0	2.1563E-8	8.1939E-5
	Max.	1.9103E-3	5.8135E-5	22.057E-2
Case 3	Min.	0	1.3011E-7	27.338E-5
	Max.	1.3783E-3	4.1001E-5	15.557E-2

continuity between the implant and the cranial model was preserved, demonstrating an appropriate reconstruction for the patient.

3.3. AM process for customized implant

The INTAMSYS Funmat HT 3D printer can be utilized for the fabrication of personalized PEEK skull implants, working on the FFF principle. FFF is one of the most unpretentious and common AM techniques. The manufacturing of 3D-printed items is controlled by numerous parameters within this method (Abdulridha et al., 2025; Hamed & Abbas, 2023). Therefore, it is essential to choose the right parameters while fabricating any component. Table 3 includes the process parameters that were implemented during the manufacture of the PEEK skull implant. The PEEK filament, which has a diameter of 1.75 millimeters, is introduced from a spool through a heated extruder head and then deposited on a platform that has been created. To generate the required form, the extruder or print head is moved in the X and Y dimensions according to the CAD model using computer control. After each layer is finished, the print head is shifted vertically in the Z-axis to begin a new layer of material. This process continues until the print is finished. Printing takes place in a sealed room with the following temperature settings: bed 130ºC, chamber 90ºC, and print 420ºC. To make a completely solid construction, the infill value in the slicing program has been adjusted to 100%. The PEEK skull implant is post-processed by the removal and detachment of its support components.

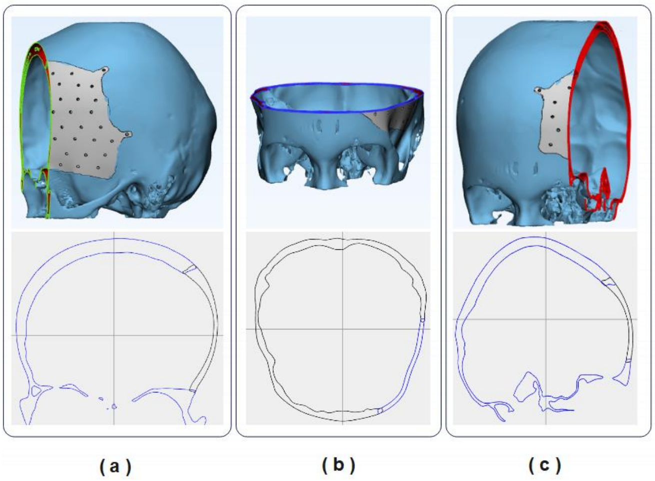

Fig. 11. The morphological fit and contour continuity assessment of the cranial implant. a) Y-axis cutting plane and sectional analysis. b) Z-axis cutting plane and sectional analysis. c) X-axis cutting plane and sectional analysis.

The printed PEEK implant with the skull model is shown in Fig. 12. For evaluation and testing purposes, a model of the skull is made from acrylonitrile butadiene styrene (ABS) utilizing the Ender 5 Pro printer. The purpose of creating the 3D model was to evaluate the virtual verification findings and ensure the general fit and congruence of the patient-specific skull implant. The implant fits exactly on the damaged skull area, offering excellent aesthetic results.

Table 3. Adjusting the parameters of the Intamsys Funmat HT 3D printer to fabricate the PEEK implant.

Description	3D Printer Settings
Printing Technique	FFF
Extruder	Single
Diameter of the extruder (mm)	0.4
The thickness of the layer (mm)	0.1
Printing speed (mm/s)	50
Diameter of filaments (mm)	1.75
Temperature of the nozzle (°C)	420
Building temperature (°C)	130
Temperature of the chamber (°C)	90

Fig. 12. 3D representation of the skull-fitting cranial implant.

3.4. Discussions

Overall, the deformation was primarily distributed around the implant's center and concentrated in close proximity to it. Simulation findings indicated that the maximum deformation value in all cases was approximately 1.9 µm. The largest displacement was observed in case 2, which was 1.9103 µm. In contrast, the maximum Von Mises strain and Von Mises stress in the cranial implant occur primarily at the edge. The maximal von Mises stress of 22.057E-2 MPa was recorded; this is lower than the PEEK yield strength of 95 MPa (Moby et al., 2022). All three cases had relatively small values for the maximal von Mises strain: 1.7135E-5, 5.8135E-5, and 4.1001E-5. For simplicity, numerical analysis was done with isotropic properties of the materials. So, the safety factor indicator is used to prove the performance and quality of the implant produced using FFF technology. The observed results indicated a very high safety factor (safety factor = yield strength / maximum stress = 95 / 22.057E-2 ≈ 431). This safety factor indicates that the implant can reliably endure physiological load even with the reduced mechanical properties in certain directions. Therefore, the results acquired maintain their reliability and validity despite the use of isotropic properties. According to the simplicity assumption of FEM, mechanical tests are not included in verifying the numerical model under study; it is verified through the safety factor relationship. Notwithstanding that limitation, results demonstrated that the implant functioned within high safety levels, therefore validating the reliability of the FEA model used.

On the other hand, the virtual matching and contour continuity of the created implants and the cranium were tested. The cross-sectional analysis indicated a high degree of uniformity in the external profile curvature contours between the cranium model and the implant. The tangency between the implant and the cranium model was preserved, demonstrating a satisfactory reconstructive fit. After reviewing the simulation results, the precision and match of the implant with the individual's cranium are shown using the 3D printing of an ABS model of the damaged region and the PEEK implant. As a result, the surgeon can assess the cranium implant's compatibility with the individual's skull and plan for the pre-surgery. Although the results supported the implant's clinical viability in terms of physiological loads. However, its long-term performance, such as infection potential, durability, and effectiveness, remains subject to further study.

4. Conclusion

This paper presents an approach for designing and evaluating cranial implants for cranial deformities. This study enhances the design precision of artificial bones, allowing surgeons and other medical personnel to closely examine the geometry of injuries and the aesthetics of implants. Additionally, it provides doctors with a visible assist for identifying and evaluating pre-surgery planning. This creates remarkable opportunities for the production of customized patients' implants. On the other hand, this approach minimizes the risk and the amount of time needed in surgery by avoiding the need for repairing parts of the implant during surgery. The suggested approach was implemented on a single-case study. The FEA model incorporated certain simplifications, including the assumption of isotropic properties of PEEK and the exclusion of print path influences. The FEM was used to analyze the cranial implant under the individual's basic operational conditions, which included an outside load of 50 N and intracranial pressure. The results of the simulation indicated that the parameter values are within the allowable range. The implant's virtual fit and contour continuity with the cranium were also analyzed. The results demonstrated a satisfactory reconstruction match, as indicated by the outstanding uniformity of the outer profile curvature contours. Lastly, the shape of the implant assures aesthetics and therefore improves the patient's quality of life. Our future work will be focused on studying printed structures of porous PEEK implants. For example, analyze the structural efficiency of the porous PEEK implants in relation to cost, weight, and strength using FEA; validate the results experimentally by mechanical testing; and compare them with solid implant structures.

Reference

Abdulridha, H. H., Obaeed, N. H., Jaber, A. S., 2025. Optimization of fused deposition modeling parameters for polyethylene terephthalate glycol flexural strength and dimensional accuracy. Advances in Science and Technology Research Journal, 19(4), 50–64. DOI: 10.12913/22998624/200088

Al-Bdairy, A. M. J., Ghazi, S. K., Abed, A. H., 2025. Prediction of the mechanical properties for 3D printed rapid prototypes based on artificial neural network. Advances in Science and Technology Research Journal, 19(3), 96–107. DOI: 10.12913/22998624/197405

Al-Wswasi, M., Al-Khaleeli, W. A., Aufy, S. A., 2025. Implement the artificial neural network concept for predicting the mechanical properties of printed polylactic acid parts. Advances in Science and Technology Research Journal, 19(5), 73–83. DOI: 10.12913/22998624/201463

Becker, L. C., Bergfeld, W. F., Belsito, D. V., Hill, R. A., Klaassen, C. D., Liebler, D. C., Marks, J. G., Shank, R. C., Slaga, T. J., Snyder, P. W., & Andersen, F. A., 2011. Final Report of the cosmetic ingredient review expert panel safety assessment of polymethyl methacrylate (PMMA), methyl methacrylate crosspolymer, and methyl methacrylate/glycol dimethacrylate crosspolymer. In International Journal of Toxicology, 30(3), 545-655. DOI: 10.1177/1091581811407352

Bhargava, D., Bartlett, P., Russell, J., Liddington, M., Tyagi, A., & Chumas, P., 2010. Construction of titanium cranioplasty plate using craniectomy bone flap as template. Acta Neurochirurgica, 152(1), 173–176. DOI: 10.1007/s00701-009-0394-2

Canac, N., Jalaleddini, K., Thorpe, S. G., Thibeault, C. M., & Hamilton, R. B., 2020. Review: Pathophysiology of intracranial hypertension and noninvasive intracranial pressure monitoring. In Fluids and Barriers of the CNS. 17(1). DOI: 10.1186/s12987-020-00201-8

de Souza Leão, R., Maior, J. R. S., de Araújo Lemos, C. A., do Egito Vasconcelos, B. C., Montes, M. A. J. R., Pellizzer, E. P., & de Moraes, S. L. D., 2018. Complications with PMMA compared with other materials used in cranioplasty: a systematic review and meta-analysis. Brazilian Oral Research, 32. DOI: 10.1590/1807-3107bor-2018.vol32.0031

Hamed, M. A., & Abbas, T. F, 2023. The Impact of FDM Process Parameters on the Compression Strength of 3D Printed PLA Filaments for Dental Applications. Advances in Science and Technology Research Journal, 17(4), 121–129. DOI: 10.12913/22998624/169468

Harrysson, O. L. A., Hosni, Y. A., & Nayfeh, J. F., 2007. Custom-designed orthopedic implants evaluated using finite element analysis of patient-specific computed tomography data: Femoral-component case study. BMC Musculoskeletal Disorders, 8(1). DOI: 10.1186/1471-2474-8-91

Huys, S. E. F., Van Gysel, A., Mommaerts, M. Y., Sloten, J. Vander., 2021. Evaluation of Patient-Specific Cranial Implant Design Using Finite Element Analysis. World Neurosurgery, 148, 198–204. DOI: 10.1016/j.wneu.2021.01.102

Jabbar, R., Alduroobi, A. A., Al-Zubaidy, S. S., 2020. Development algorithms for points cloud pre-processing. 2nd International Conference on Materials Engineering & Science (IConMEAS), Baghdad, Iraq, 020081.

Jindal, S., Manzoor, F., Haslam, N., & Mancuso, E., 2021. 3D printed composite materials for craniofacial implants: current concepts, challenges and future directions. The International Journal of Advanced Manufacturing Technology, 112(3), 635-653. DOI: 10.1007/s00170-020-06397-1/Published

Kung, W. M., Tzeng, I. S., Lin, M. S., 2020. Three-dimensional CAD in skull reconstruction: A narrative review with focus on cranioplasty and its potential relevance to brain sciences. Applied Sciences, 10(5), 1847. DOI: 10.3390/app10051847

Lalegani Dezaki, M., Mohd Ariffin, M. K. A., Hatami, S., 2021. An overview of fused deposition modelling (FDM): Research, development and process optimisation. Rapid Prototyping Journal, 27(3), 562–582. DOI: 10.1108/RPJ-08-2019-0230

Lee, W. T., Koak, J. Y., Lim, Y. J., Kim, S. K., Kwon, H. B., Kim, M. J., 2012. Stress shielding and fatigue limits of poly-ether-ether-ketone dental implants. Journal of Biomedical Materials Research - Part B Applied Biomaterials, 100 B(4), 1044–1052. DOI: 10.1002/jbm.b.32669

Liu, Y., Yi, N., Davies, R., McCutchion, P., Ghita, O., 2023. Powder Bed Fusion Versus Material Extrusion: A Comparative Case Study on Poly-ether-Ether-Ketone Cranial Implants. 3D Printing and Additive Manufacturing, 10(5), 941–954. DOI: 10.1089/3dp.2021.0300

Luo, C., Liu, Y., Peng, B., Chen, M., Liu, Z., Li, Z., Kuang, H., Gong, B., Li, Z., Sun, H., (2023. PEEK for Oral Applications: Recent Advances in Mechanical and Adhesive Properties. In Polymers, 15(2), 386. DOI: 10.3390/polym15020386

Mandolini, M., Brunzini, A., Brandoni Serrani, E., Pagnoni, M., Mazzoli, A., Germani, M., 2019. Design of a custom-made cranial implant in patients suffering from Apert syndrome. Proceedings of the Design Society: International Conference on Engineering Design, Delft, The Netherlands, 709–718.

Mansor, K. K., Shabeeb, A. H., Hussein, E. A., Abbas, T. F., Bedan, A. S., 2024. A statistical investigation and prediction of the effect of FDM variables on flexural stress of PLA prints. Tikrit Journal of Engineering Sciences, 31(3), 10–17. DOI: 10.25130/tjes.31.3.2

Mejía Rodríguez, M., González-Estrada, O. A., Villegas-Bermúdez, D. F., 2024. Finite Element Analysis of Patient-Specific Cranial Implants under Different Design Parameters for Material Selection. Designs, 8(2), 31. DOI: 10.3390/designs8020031

Moby, V., Dupagne, L., Fouquet, V., Attal, J. P., François, P., Dursun, E., 2022. Mechanical Properties of Fused Deposition Modeling of Polyetheretherketone (PEEK) and Interest for Dental Restorations: A Systematic Review. In Materials, 15(19), 6801. DOI: 10.3390/ma15196801

Moiduddin, K., Darwish, S., Al-Ahmari, A., ElWatidy, S., Mohammad, A., Ameen, W., 2017. Structural and mechanical characterization of custom design cranial implant created using additive manufacturing. Electronic Journal of Biotechnology, 29, 22–31. DOI: 10.1016/j.ejbt.2017.06.005

Moncayo-Matute, F. P., Vázquez-Silva, E., Peña-Tapia, P. G., Torres-Jara, P. B., Moya-Loaiza, D. P., Viloria-Ávila, T. J., 2023. Finite Element Analysis of Patient-Specific 3D-Printed Cranial Implant Manufactured with PMMA and PEEK: A Mechanical Comparative Study. Polymers, 15(17), 3620. DOI: 10.3390/polym15173620

Neamah, Z. H., Al-Kindi, L. A. H., Al-Kindi, G., 2024. ABC model for cost estimation of custom implants by Additive Manufacturing. PLoS ONE, 19(5). DOI: 10.1371/journal.pone.0301440

Obaeed, N. H., & Hamdan, W. K., 2024. Cranioplasty materials for human skull rehabilitation. Advancements in Sustainability Systems, Nova Science Publishers, Hauppauge, NY, USA.

Petersmann, S., Smith, J. A., Schäfer, U., Arbeiter, F., 2023. Material extrusion-based additive manufacturing of polyetheretherketone cranial implants: Mechanical performance and print quality. Journal of Materials Research and Technology, 22, 642–657. DOI: 10.1016/j.jmrt.2022.11.143

Punchak, M., Chung, L. K., Lagman, C., Bui, T. T., Lazareff, J., Rezzadeh, K., Jarrahy, R., Yang, I., 2017. Outcomes following polyetheretherketone (PEEK) cranioplasty: Systematic review and meta-analysis. In Journal of Clinical Neuroscience, 41, 30-35. DOI: 10.1016/j.jocn.2017.03.028

Ridwan-Pramana, A., Marcián, P., Borák, L., Narra, N., Forouzanfar, T., Wolff, J., 2016. Structural and mechanical implications of PMMA implant shape and interface geometry in cranioplasty - A finite element study. Journal of Cranio-Maxillofacial Surgery, 44(1), 34–44. DOI: 10.1016/j.jcms.2015.10.014

Saleh, A. M., Jaber, A. S., Jabbar, M. S., 2025. Layer adhesion investigation of three dimension printed parts by controlling the environment temperature. Advances in Science and Technology Research Journal, 19(3), 74–83. DOI: 10.12913/22998624/197333

Shiaa, W. Q., Abdulghafour, A. B., Hassoon, O. H., 2023. A Novel Method Based on Interpolation for Accurate 3D Reconstruction from CT Images. International Journal of Intelligent Engineering and Systems, 16(2), 506–516. DOI: 10.22266/ijies2023.0430.41

Shiaa, W. Q., Abdulghafour, A. B., Hassoon, O. H., 2024a. 3D reconstruction from CT images utilizing the open-source tool. The fourth Al-Noor International Conference for Science and Technology (4NICST2022), Istanbul, Turkey, 060024.

Shiaa, W. Q., Abdulghafour, A. B., Hassoon, O. H., 2024b. An enhanced technique for removing soft tissues and highlighting regions of interest in medical images. The 3rd International Conference on Electromechanical Engineering & its Applications (ICEMEA-2022), Baghdad, Iraq, 020005.

Singh, S., Prakash, C., Ramakrishna, S., 2019. 3D printing of polyether-etherketone for biomedical applications. In European Polymer Journal 114, 234-248. DOI: 10.1016/j.eurpolymj.2019.02.035

Sonaye, S. Y., Mack, J. P., Tan, K. T., Owusu-Danquah, J. S., Sikder, P., 2025. A comprehensive analysis of high-temperature material extrusion 3D printing parameters on fracture patterns and strength of polyetheretherketone cranial implants. Progress in Additive Manufacturing, 10(1), 927–942. DOI: 10.1007/s40964-024-00688-9

Trevisan, F., Calignano, F., Aversa, A., Marchese, G., Lombardi, M., Biamino, S., Ugues, D., Manfredi, D., 2018. Additive manufacturing of titanium alloys in the biomedical field: processes, properties and applications. In Journal of Applied Biomaterials and Functional Materials, 16(2), 57-67. DOI: 10.5301/jabfm.5000371

Zanjanijam, A. R., Major, I., Lyons, J. G., Lafont, U., Devine, D. M., 2020. Fused filament fabrication of peek: A review of process-structure-property relationships. In Polymers, 12(8), 1665. DOI: 10.3390/POLYM12081665